Article

Not peer-reviewed version

# Control Method of Load Sharing between AC Machine and Energy Storage Bank in the DC Grid

Maciej Kozak *, Maciej Słodkowski , Seweryn Sawicki

Posted Date: 1 February 2024

doi: 10.20944/preprints202402.0061.v1

Keywords: Active circuits; bridge circuits; microgrids; power distribution; pulse width modulation

*Article*

# Control Method of Load Sharing between AC Machine and Energy Storage Bank in the DC Grid

**Maciej Kozak [1,*], Maciej Słodkowski [2] and Seweryn Sawicki [3]**

[1] Maritime University of Szczecin; m.kozak@pm.szczecin.pl
[2] Maritime University of Szczecin; 29870@s.pm.szczecin.pl
[3] Maritime University of Szczecin; 29868@s.pm.szczecin.pl
* Correspondence: m.kozak@pm.szczecin.pl

**Abstract:** The article presents the issues related to load sharing in direct current grid and a novel control method which has advantages over known solutions. Unlikely of many similar sounding papers this article shows attempt of creation fully controllable non-isolated system which allows load sharing between permanent magnet alternator equipped with machine side converter (MSC) and dual active bridge (DAB) tied to batteries or supercapacitor. The power sharing is essential feature of parallel connected direct current generators and all types of voltage sources in this way are contributing power to the system. Such system should have possibility of the rapid voltage build up in the case of sudden electrical load changes. To keep the optimal efficiency of the alternator the rotational speed changes according to proper mapping of driving combustion engine. When rotational speed is too low then sudden electrical load can cause significant voltage drop and time needed for voltage build up will vary according to RPM increase. In such situations the undervoltage system can trip the breaker and finally there may be a blackout. To avoid such problem the DC systems which consist of batteries and supercapacitor were introduced. System components include a self-excited synchronous generator (SESG) operating at variable shaft speed as well as batteries and supercapacitors that provide electricity for sudden electrical load changes on the distribution grid. The core of presented system is in power distribution method which consists of programmed controllers structure allowing precise currents distribution. A novelty in the proposed method is the use of a cascaded system of current and DC voltage regulators which allows power distribution precise control. In contrary to previously presented solutions, the proposed system allows fast and accurate control of currents loading parallel connected DC voltage sources for wide range generator speed changes. In presented solution both converters have been equipped with Schottky diodes preventing flow of equalizing currents between closed transistors in the parallel mode of operation. An experimental test-stand of the described system is presented with its theoretical basis and experimental results.

**Keywords:** active circuits; bridge circuits; microgrids; power distribution; pulse width modulation

## 1. Introduction to direct current grids and power sharing issues

The global renewable and clean energy challenges became a driving force of the renewable energy sources development. There are many ways to achieve higher effectiveness off widely used renewable sources but not all of them can be used onboard of seagoing ships. These solutions must apply rules and regulations which are quite strict when it comes to ensuring power supply continuity thus distribution of electrical load. Because of that and accordingly to new environmental pollution demands a lot of effort is being done in to make the most effective use of existing solutions. These include different types of power plants topologies and electrical grids with solutions incorporating direct current distribution systems with based on efficient network technologies namely the microgrids used both on vessels and in inland [1,2,3]. Researchers are becoming increasingly interested in industrial installations and electro-mobile systems. Interestingly DC networks are more

 doi:10.20944/preprints202402.0061.v1



flexible than widely used alternating current installations, are smaller of about 30% and can be successfully used in marine power systems. There are some drawbacks arising from direct current technology but still a lot of efforts is being done on preparation of robust systems which have all features required in electrical power grids. The regular island mode power grid (isolated from external sources) system which is dominant on the board of the vessels must meet many requirements e.g., a stable asymmetrical load sharing feature with maintain appropriate voltages levels which has been shown in [4,5]. Another important advantage of such systems is possible use of electricity storage banks consisting of batteries and ultra/supercapacitors. These solutions can reduce fuel consumption and pollutant emissions. This is typical stand-alone system, made of active and passive sources and in the naval architecture the energy comes mostly from non-renewable resources (diesel generators), energy storage systems (ESS) and power electronics converters [6]. Operation of such in reference to microgrids is called islanding mode and it means such a system can run off-grid but there is also possibility of cold-ironing while stay at berth [7,8]. This kind of solution gives the control of individual sources feeding consumers by appropriate power distribution algorithm. The paper presents theoretical assumptions and experimental results of an original power distribution system consisting of a variable-speed rotating synchronous alternator, a battery with a bidirectional DC-DC converter and a super capacitor bank switched with batteries pack improved to earlier version of similar system presented in [4] and [9]. The batteries and supercapacitors are a buffer to store excess energy and deliver it back to the system when needed just to keep operational parameters at optimal level.

A summary of the solutions of an energy storage system is presented in [10], along with significant features. The electrical power balance in an electrical weak network varies greatly based on the momentary changes in the power flow. High-frequency components can be suggested due to the dynamics of power exchange processes. Whenever large consumers are switched on or a shaft generator produces energy intermittently while propeller emerge out of the water, power demand can spike quickly. On the other hand, the low-frequency components, such as the average daily energy consumption pattern, can be noticed. Fast reaction time components are typically required for high-frequency and quick changes in power consumption whereas the electrochemical batteries, on the other hand, offer high energy density for low-frequency components.

A bidirectional AC-DC converter with capacitors and batteries was used in long-term parallel operation of a synchronous generator. Such a system connected to the grid through an isolated DC-DC converter offered fast reaction to sudden load changes and the working tests are presented in this work. Two converters were connected by direct current intermediate circuits in such a way that the load sharing of the two sources could be adjusted, resulting in an improved combustion engine operation.

## 2. Proposed system topology and features

To effectively connect two or more direct voltage regular, shunt excited generators and distribute power between them mostly the voltage droop method is utilized [11]. This system uses generators excitation current control coming from automatic voltage regulator and by its real-time control the voltage produced on the terminals is precisely controlled. The droop power sharing conception comes from direct currents generators which was widely used in such systems [12]. Main idea behind the voltage droop control is in proper excitation current balancing so the resulting terminal voltage of DC generators can be changed by a small amount. This little variation can result in notably high load takeover by a generator producing higher voltage. There are means provided to control the voltage on the parallel connected other generator which allow simultaneous control over voltages in the system and amount of power taken by both generators. Such system seems to be very simple but behind the simplicity there are hidden features which can give a hint for modern, power electronics-based DC grids development.

To connect the active and passive voltage sources the topology shown in the Figure 1 was utilized. The pack of batteries and supercapacitor as passive sources were used while active source was synchronous generator with line side inverter. As it can be seen the voltage sources (of negligible

 doi:10.20944/preprints202402.0061.v1



internal impedance) are separated because of auctioneering diodes use which restrict flow of circulating currents. These currents in turn would prevent correct power distribution and cause uncontrolled flow of currents with values dependent on source impedance. The principle of operation of the system consists in continuous changes of the values of the set voltages $U_{dc1}$ and $U_{dc2}$ so that the diodes of the AC/DC machine inverter and the DC/DC converter switch from the blocking state to the conduction state and enable the flow of the current sustaining the set voltage of the DC network $U_{dc}$. As it is known, diodes are not perfect switches and in this special mode of auctioneering operation their properties become important. The most relevant in this very application is the reverse recovery current flow while transient time from conduction to the off state. The explanation of such is as follows. In the case of changing polarity or when reverse voltage is applied to the diode forward current flow stops, reverse current (recovery current) shows up for an instant. The recovery current value may oscillate depending on the conditions of use. Ringing is another term for this oscillation. The time it takes for a switching diode to turn totally off from an on state is referred to as the reverse recovery time, or $t_{rr}$. Electrons cannot generally be halted immediately once an operation is turned off, resulting in some current flow in the opposite direction. The larger the loss, the higher the leakage current. Metal diffusion, material optimization, and the development of fast recovery diodes that decrease ringing after recovery can all help to reduce reverse recovery time but for proposed application these are not applicable yet for technical reasons.

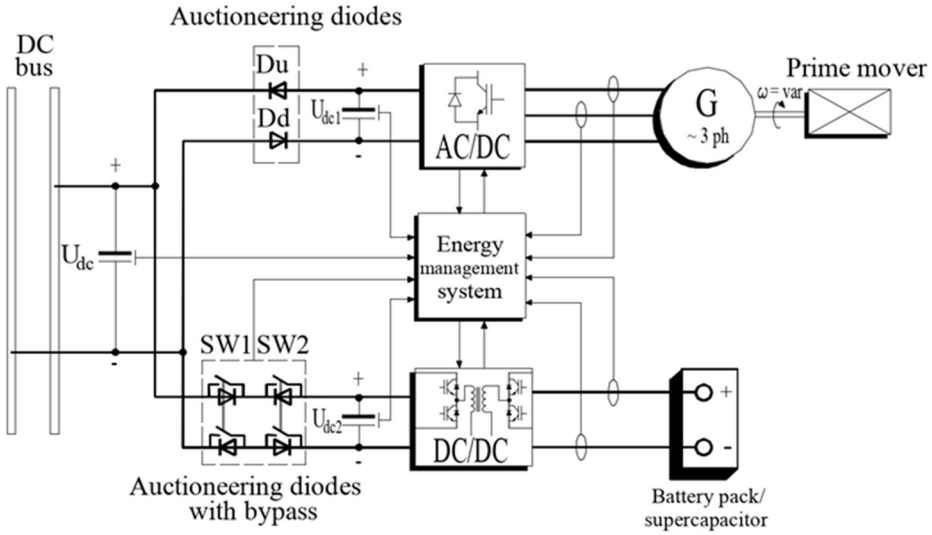


**Figure 1.** The intermediate circuits of parallel operating machine-inverters and DC-DC converters connected through auctioneering diodes.

*2.1. The control principles of the proposed system*

Presented system contains two main functional elements which can work separately or in parallel. These units are controlled independently and work asynchronously from each other. First control algorithm implemented in a dual active bridge controls DC voltage and keeps it on the fixed level. The DAB inner control loops can be preprogrammed to operate in one of the three modes:

- charging batteries,
- discharging energy storage,
- discharging with control and maintain of DC output.

In the third mode of operation system is precisely tuned just to maintain resulting DC bus voltage and allows work along other DC voltage sources in parallel connection. In the proposed system this DC-DC unit is considered as the "master" which keeps the voltage level in the power distribution mode and draws energy from the batteries or supercapacitor. It can be easily programmed to work in the bus voltage following mode with active current limiting but this feature is not covered in the paper. This kind of operation in DC microgrids is known as master mode [13]

 doi:10.20944/preprints202402.0061.v1



when selected source keeps the voltage on constant level and forces other to follow the voltage value within current limits. The energy management system should control operation of such and affect power distribution in the case of energy storage voltage drop below operational range. Another reason why DAB was chosen as superior system is that the converter works with batteries, which are sources of relatively voltage slow changes compared to the MSC where the rotational speed can be quickly changed thus back emf and generated voltage. This feature makes MSC control loops tuned to be prone to such disturbances and sometimes this kind of erratic behavior may arise control instabilities especially in the systems with number of active sources [14].

Because of the aforementioned reasons machine side inverter was chosen as more convenient. The main control loop could be modified easily to use as the following source in the power sharing mode.

On the other hand, in the independent mode of operation of machine and its inverter main control loop keeps the DC voltage constant on the output and operates in wide range of currents up to the nominal value. The main nonlinear controller operates with different proportional coefficients according to the varying error signal value. For these values calculated in reference to the actual DC bus voltage, a set of coefficients is taken from the look-up table and inserted online into the software controllers.

As it can be seen in the Figure 2 the difference between commanded DC voltage and its actual value can change rapidly due to turn on heavy consumer into the operation thus significant direct voltage drop. This causes proportional component to raise quickly which affects control accuracy leading to overshoot. In the islanding mode these values should be limited mainly not to exceed the permissible values which are given in [15] and to keep required dynamics.

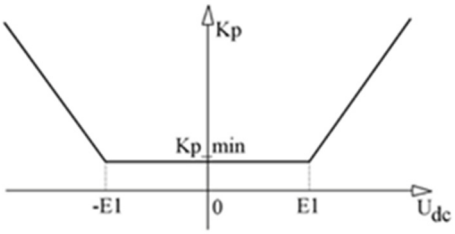


**Figure 2.** Nonlinear relationship of proportional component P gain Kp_min with DC voltage error value E1.

Things, however, are getting more complicated when it comes to parallel operation of the voltage sources of small impedance. In such arises problem of very precise DC voltage regulation in order to obtain proper direct current sharing between controlled voltage sources.

In parallel operation even slight inaccuracy of DC voltage regulation causes large differences in power distribution and, in case of low control accuracy (or notable Udc error), can prevent from demanded load sharing. Because of that the machine side inverter control method should become more precise when there is a need to power distribution between voltage sources in parallel operation.

### *2.2. Synchronous generator and DC-DC converer output stage control principles*

Control of self excited generator involves regulating frequency and voltage by adjusting active and reactive power. In the generating sets arrangement, a combustion engine provides active power, while excitation windings current ensures reactive power. A rotational speed governor and automatic voltage regulator provide data for the two independent control loops. Simple, straightforward scalar control procedures like this omit some phenomena, such as the coupling effect between synchronous generator electrical axes [16]. Among the many suitable methods for this purpose is field orientation vector control. Since AC machines use vector control, their performance during transient operation modes is quite similar to that of direct current machines. Space-phasor theory provides the mathematical foundation for the dynamic model and vector control of AC

Preprints.org (www.preprints.org) | NOT PEER-REVIEWED | Posted: 1 February 2024 doi:10.20944/preprints202402.0061.v1



machines [17]. A rotor flux oriented synchronous machine model can be used to simulate DC generator operation, but a field oriented model is used for controlling the generator. In a sense, this concept resembles a DC machine in which the two variables are controlled independently to produce electromechanical torque. The DC machine equipped with commutator produces top torque in comparison with almost any AC machine due to its mechanical alignment of the commutator thus the perpendicular orientation of armature current and a stator flux. Nowadays such case is not considered because of certain problems arising from the brushes and commutator and it can be stated that only brushless machines are in use in maritime industry today.

In the synchronous generator the stator currents and magnetic fluxes depicted in Figure 3 are given by:

$$i_s = i_{sd} + j i_{sq} \tag{1}$$

$$\begin{aligned} \Psi_{sd} &= -\int \left(v_{sd} + R_s i_{sd} + \omega_e \Psi_{sq}\right) dt \\ \Psi_{sq} &= -\int \left(v_{sq} + R_s i_{sq} - \omega_e \Psi_{sd}\right) dt \end{aligned} \tag{2}$$

where: $\Psi_{sd,}$ and $\Psi_{sq}$ are the stator fluxes in d-q plane and $\omega_e$ is the stator magnetic flux rotational speed.

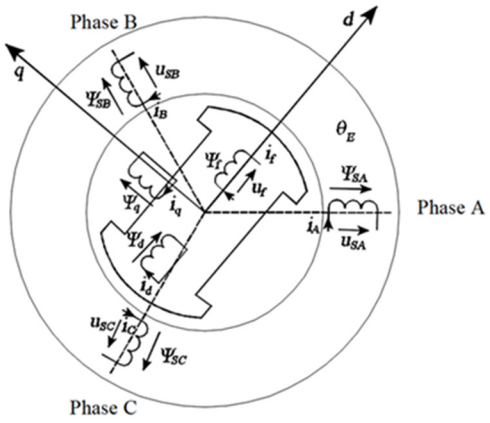


**Figure 3** Simplified scheme of the 2 poles SESG with rotor and stator fluxes in d-q axis depicted.

Quadrature in the generating mode determines active power and intermediate circuit voltage and, due to reversed energy flow, is negative. The flux component is also negative due to its demagnetizing properties and corresponds to the reactive power generated. An active current component creates torque by influencing the exciting current. Field oriented exciting currents have a longitudinal component due to decoupled control, which contributes to their magnetizing properties.

For power flow to be controlled, the stator current must be oriented in the direction of the magnetizing flux which is implemented in a control algorithm using Clarke and Park ($\alpha$-$\beta$ and $d$-$q$) plane transformations. A constant torque angle control strategy maintains the current vector on the $q$ axis aligned with the current vector on the $d$ axis at all times. Considering both $i_{sd}$ and $i_{sq}$ currents in a synchronous generator, the torque equation is as follows:

$$T_e = \frac{3}{2} p\left[\Psi_m i_{sq} + \left(L_{sd} - L_{sq}\right) i_{sq} i_{sd}\right] \tag{3}$$

where: $\Psi_m$ is field winding flux, $p$ is the number of pole pairs and $L_{sd}$ and $L_{sq}$ are values of the stator self inductances. As a result of some simplifications, the torque equation becomes:

$$T_e = \frac{3}{2} p \Psi_m i_{sq} \tag{4}$$

Because machine torque and active current are linearly related, equation (4) shows that the generator can be controlled by means of stator current and flux mutual regulation. In the $d$-$q$ coordinates, the $i_{sq}$ independent control loop assures that the DC intermediate circuit voltage $U_{dc}$ is

 doi:10.20944/preprints202402.0061.v1



always a non-zero value even when the reactive current $i_{sd}$ equals to zero. As it can be seen in Figure 3 to control PWM inverter the signals of *d-q* plane voltages are applied. To achieve such there is a need to translate current signals into the voltages. From a theory this conversion is done with following dependencies coming from (2):

$$v_{sd} = R_s i_{sd} + L_{sd}\frac{di_{sd}}{dt} - \omega_r L_{sq} i_{sq} \tag{5}$$

$$v_{sq} = R_s i_{sq} + L_{sq}\frac{di_{sq}}{dt} + \omega_r L_{sd} i_{sd} + \omega_r \Psi_m \tag{6}$$

where $v_{sd}$ and $v_{sq}$ are the d-axis and q-axis stator terminal voltages and $R_s$ describes the resistance of the stator phase windings.

In (6) substituting term $\omega_r \Psi_m$ which describes back EMF with E and applying a Laplace transform we get:

$$v_{sq} - E = R_s i_{sq} + L_{sq}\frac{di_{sq}}{dt} + \omega_r L_{sd} i_{sd} \tag{7}$$

In the FOC control method applied in this case the magnetizing current $i_{sd}$ is kept at 0 (by decoupling term) so the part including active current in (7) can be canceled thus the transfer function of the machine is given by:

$$\frac{i_{sq}}{v_{sq} - E} = \frac{1}{sL_{sq} + R_s} \tag{8}$$

Introducing electrical time constant $\tau_{sq} = \frac{L_{sq}}{R_s}$ in (8) yields

$$\frac{i_{sq}}{v_{sq} - E} = \frac{1}{R_s(s\,\tau_{sq} + 1)} \tag{9}$$

In the presented solution a sensorless system was utilized to obtain rotational speed and stator field angle values needed for Clarke and Park transformations. This control method utilizes flux angle calculation block which takes information from observer which in fact is a block of the DSP software running real-time parallel with machine. The current values used in the flux calculation block are filtered out due to noise coming from current sensors, so it provides smooth operation of the control system. The speed calculation equations are fed with measured current values and known voltages applied to the windings. This allows calculation of flux in reference $\alpha$-$\beta$ plane which in turn leads to reference frame angle calculation. This is needed to provide information for forward and inverse Park transformation crucial in FOC control and can be useful in rotational speed estimation.

There are three main control loops in the proposed structure: the DC voltage outer loop and the active along with magnetizing current fast loops (in Figure 4 denoted as $i_{sq}$ and $i_{sd}$ currents) which is consistent with the classical FOC scheme. Besides providing long-term voltage regulation for DC intermediate circuits, the field oriented control technique also enables the distribution of power between parallel DC sources thanks to introducing active current limitations. What distinguishes the presented method from classical solutions is presence of the fourth PI control loop which produces signal denoted as $U_{corr}$. In the islanding mode of operation, the DC link voltage is main controlled quantity, so the regulators parameters are tuned for dynamics of such. Regarding the active current limitation correcting voltage signal provides power distribution instead of limiting $i_{sq}$ current in the main loop which should be set to the nominal value of the machine and inverter value. The correction loop is enabled in the case of parallel operation and can be limited not to exceed safe operation area of the inverter's DC intermediate circuit voltage. This additional control loop eliminates nonlinear regulators moreover enables precise and fast voltage control when power distribution mode is required. As it may be deduced additional corrector control loop should be used in parallel operation mode limiting active current contribution to the consumer. Another important issue is parameter variations occurring during system operation. Proposed parallel connected system inherently is not ideally stiff which means that both sources cannot keep intermediate voltages on the required level in the operational range. In the case of simple DC voltage control, fluctuations of the intermediate

 doi:10.20944/preprints202402.0061.v1



voltage generated by the DAB contributing to incorrect power distribution. It follows from the methodology of a system without an additional regulator that, in order to be able to limit the current, the DC bus control voltage must be increased by adding a certain value to the reference level. This value should depend on the current state of the bus voltage so that the load current distribution can be precisely regulated. Because in the parallel operation the voltage measurements are common for DC bus and intermediate circuits connected these values cannot be precisely determined without active currents control.

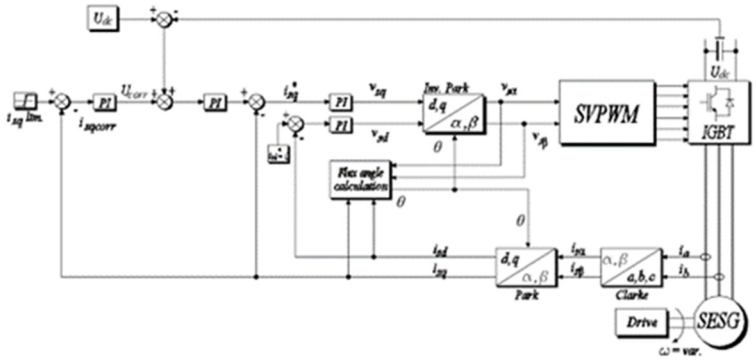


**Figure 4**. Scheme of the self excited synchronous generator field oriented sensorless control with flux angle calculation.

In the Figure 5 there is presented situation of unequal voltage intermediate circuits in two cases. In the Figure 5 a) the control over DC voltage relies solely on the main loop PI control while in the Figure 5 b) the compensating controller was used. In the time of bus voltages equalization the system without active compensator does not take any action when the current drops below limit thus the power sharing operation is not maintained. Such unfavorable situation leads to conclusion that the reference voltage setpoint should be changed either on the master or the slave controlled voltage source every time power sharing is needed. In such condition the only way to determine shared load ratio between paralleled sources is by active currents control so the additional compensator loop is necessary. Over a limited range of parameters, proposed method uses a PI controller configuration and a first-order plus dead time model. Further, all approaches involve tuning cascade control systems in two steps: first, the secondary controller is tuned based on the dynamic model of the inner process; second, the primary controller is tuned based on the dynamic model of the outer process, including the secondary loop. Consequently, if the secondary controller is retuned for some reason, an unfavorable identification step can result in an additional retune process for the primary controller.

a)

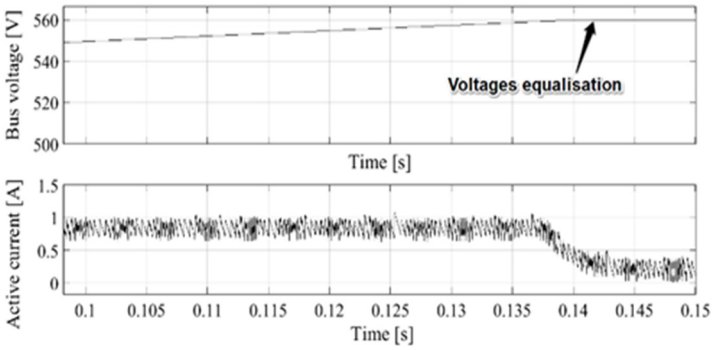

Preprints.org (www.preprints.org) | NOT PEER-REVIEWED | Posted: 1 February 2024 doi:10.20944/preprints202402.0061.v1



b)

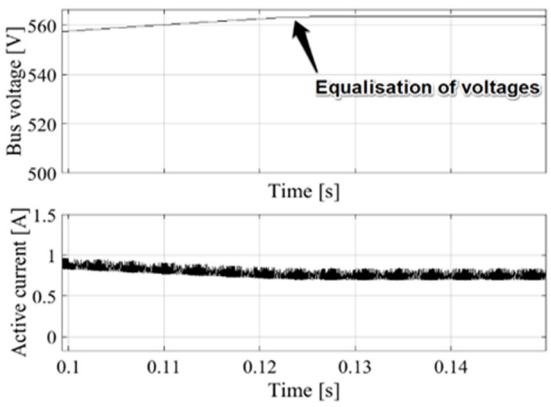


**Figure 5**. Voltages and active currents waveforms a) without compensator and b) with proposed compensator. Active current limit set to 0.8A.

*2.3. Synchronous generator dc voltage cascaded control*

One method allowing precise control is proposed, modified control closed loop enhanced in comparison to basic current regulator form with additional corrector controller. According to the Figure 4 cascaded control loop part can be presented as follows.

where: $U_{dc}$ bus is actual voltage value of DC bus, $U^{*}_{errdc}$ is the voltage error differential signal, $U_{corr}$ voltage correcting signal, $i_{sqlim}$ denotes active current limit, $i_{sqcorr}$ is the corrector current, *G1*, *G2*, *G3* are PI controllers, *H1* is the generator plant and *H2* is the external circuits block.

The control loop consists of SESG plant *H1* block which can be presented as follows:

$$H1 = \frac{1}{R_s\left(\frac{L_{sq}}{R_s}\cdot s + 1\right)} \tag{10}$$

The block *H2* describes external circuits which in presented circuit include capacitances and resistances of common DC bus bar.

$$H2 = \frac{R_{ext}}{R_{ext}\cdot C_{ext}\cdot s + 1} \tag{11}$$

where $R_{ext}$ and $C_{ext}$ are the external circuits resistances and capacitances.

The PI controllers are responsible for control signals of DC voltage outer loop, internally calculated active current and the corrector current. The auxiliary measured variable is an active current $i_{sq}$ which feeds the DC bus consumers and is crucial to maintain the proper value of direct voltage. At the same time the value of the $i_{sq}$ is critical for the sharing load control method. The current limit value comes from energy management system and fulfills the load sharing requirements which means the control of outer loop main measured variable rely solely on active current limiting.

The scheme shown in Figure 6 depicts dependencies between controlled variables, PI controllers and the active current limiter.

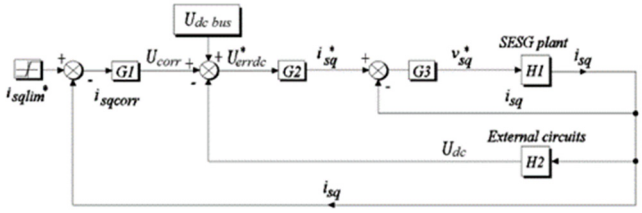


**Figure 6**. Configuration of enhanced closed-loop active current cascaded control system with corrector.

In the presented loop, the controlled and corrected variable is the active current $i_{sq}$. This current charges intermediate circuit capacitors and parallelly powers up external circuits. According to

 doi:10.20944/preprints202402.0061.v1



Figure 6 the equations describing inner control loop of active current and resulting DC voltage (all components are in the s-domain) can be expressed as:

$$i_{sq} = \left(i_{sq}^{*} - i_{sq}\right) \cdot G3 \cdot H1 \tag{12}$$

Thus:

$$i_{sq} = \frac{i_{sq}^{*} \cdot G3 \cdot H1}{1 + G3 \cdot H1} \tag{13}$$

The outer, voltage control loop can be presented as:

$$U_{dc} = U_{errdc}^{*} \cdot G2 \cdot \frac{G3 \cdot H1}{1 + G3 \cdot H1} \cdot H2 \tag{14}$$

From Figure 6 the voltage error signal is as follows:

$$U_{errdc}^{*} = U_{dc\,bus} + U_{corr} - U_{dc} \tag{15}$$

After applying (15) into (14) we get:

$$U_{dc} = (U_{dc\,bus} + U_{corr}) \frac{G2 \cdot \frac{G3 \cdot H1}{1 + G3 \cdot H1} \cdot H2}{1 + G2 \cdot \frac{G3 \cdot H1}{1 + G3 \cdot H1} \cdot H2} \tag{16}$$

In the proposed solution the error voltage along with *G2* controller signal gives the information proportional to required active current. In the slave loop commanded active current is compared to actual value and the result is transformed to machine side inverter voltages. Such a structure is used widely in control applications regarding real-time machines control and works flawless in the single mode of operation. Presented configuration refers to the cascaded control and is functional enhancement of a single loop control. The quality and performance of the cascaded control loop mainly depends on parameters [18] and coefficients of master and auxiliary loops controllers. In theory for such cascaded systems the frequency response methods are used to set the controllers properly [19]. Open loop transfer function of the main loop has higher order dynamics than inner loop in the control algorithm. There are available tuning charts allowing prediction of the master controller settings for minimizing integral of time-weighted absolute error due to load disturbances on the secondary loop in cascade control systems. Because of the use of controllers one needed information deals with stability of the system and can be obtained with means of classic analysis in s-domain. To achieve such, the transfer function of the control loops should be defined. After some simplifications on voltage equations (5,6) the transfer functions of current loops for SESG are as follows:

$$Tf_q(s) = \frac{1}{s \cdot L_{sq} + R_s} = \frac{1}{R_s\left(s \cdot \frac{L_{sq}}{R_s} + 1\right)} \tag{17}$$

$$Tf_d(s) = \frac{1}{s \cdot L_{sd} + R_s} = \frac{1}{R_s\left(s \cdot \frac{L_{sd}}{R_s} + 1\right)} \tag{18}$$

where *s* is the complex variable.

Having the parameters of the real-time system, such as computational delays and circuit time constants, it is possible to put together a control system loop without corrector.

The detailed active current control loop in its generic form is shown in the Figure 7. The active current set point is compared with its measured value and the error signal feeds PI controller. The PI controller in continuous domain transfer function according to [20] can be expressed as:

$$PI = k_{p_\omega} \frac{1 + \tau_\omega \cdot s}{\tau_\omega \cdot s} \tag{19}$$

Preprints.org (www.preprints.org) | NOT PEER-REVIEWED | Posted: 1 February 2024 doi:10.20944/preprints202402.0061.v1



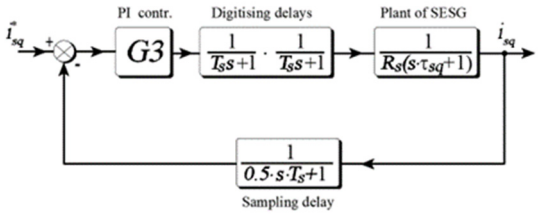


**Figure 7**. Configuration of closed-loop active current control system.

In order to obtain unitary feedback the control loop from Figure 7 can be rearranged and presented in the following figure.

To get required transfer function the input function 0.5sTs+1 should be approximated and presented in more convenient form which is $\frac{1}{1-0.5T_S s}$. The way to achieve this is to linearize this function around fixed point described as (x0, y0) = P(0, f(0)) = P(0,1).

The equation of the tangent in the general case has the form $y - y_0 = m(x - x_0)$, while $m = f'(x)|_{x=x_0} = -\frac{1}{(1-x)^2} \cdot (-1)\Big|_{x=x_0} = 1$. In the given situation $y = m(x-0) + 1 = x + 1$ and finally we have an approximation of $\frac{1}{1-x} \approx x + 1$.

After inserting the transfer functions of plant *H1* and *H2* along with *G2* and *G3* controllers given by (18) into (14) and including required calculation along with the digitizing delays the stability of the cascaded control loop has been proven.

The transfer functions have been implemented to Matlab software and for the chosen set of parameters the obtained step response is as in the Figure 10.

It should be pointed out that tuning process is crucial in order to get needed step response from designed system and values which work flawless in digital simulation probably would need some more work in digitally controlled laboratory setup.

The control signal goes to the real-time DSP-FPGA control system which introduces digitizing and calculation delays and SESG itself also has delay which mainly depends on the electric constant of investigated machine depicted in the Figure 8 as $\tau_{sq}$. This value was calculated on basis of the data acquired in the previous projects regarding investigated machine. Based on machine parameters and control system properties the open loop transfer function was created and after applying modulus optimum criterion [21] the proportional gain of the active current controller was determined. All data were included into control loop what allowed plot Bode diagram of the investigated open-loop system.

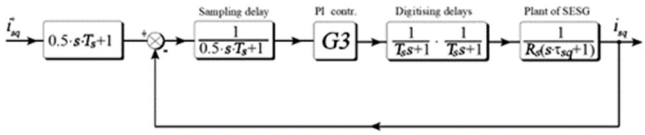


**Figure 8**. Configuration of unitary closed-loop active current control.

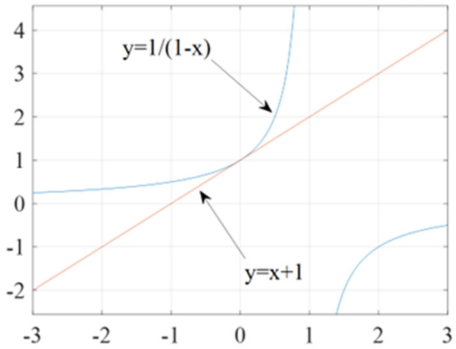


**Figure 9**. Configuration of unitary closed-loop active current control.

Preprints.org (www.preprints.org) | NOT PEER-REVIEWED | Posted: 1 February 2024 doi:10.20944/preprints202402.0061.v1



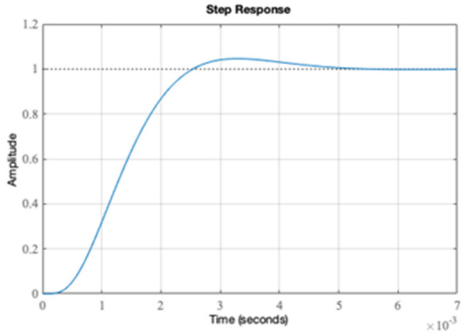


**Figure 10**. The step response of voltage controller with corrector.

For given data of machine parameters it can be read from the Bode diagram in the Figure 11 that the phase margin equals to 62.5 deg while gain margin is 13.6 dB and both are stable for closed control loop.

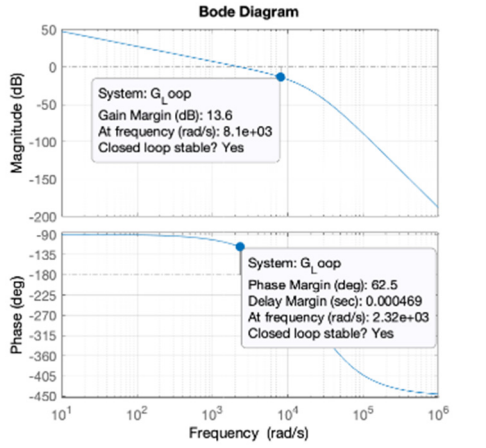


**Figure 11**. Bode plot of the active current $i_{sq}$ control loop.

Similar calculations and tests were performed to obtain information of stability in the $i_{sd}$ current loop and $U_{dc}$ based on (16) so the stability of the control was proved.

*2.4. Synchronous generator and DC-DC converer output stage control principles*

In addition to the synchronous generator inverter the complete system includes a bidirectional converter tied to the batteries pack or supercapacitors.

In the Figure 10 there is a complete system of DC-DC dual active bridge converter presented. As it can be noted DAB contains low voltage (LV) and high voltage (HV) side which are galvanically separated with high frequency (HF) transformer. This ensures lack of dependency between closing transistors on both sides of converter. The dual active bridge utilizes two modes of operation. In the first mode converter charges batteries and a combination of switches denoted as SW1 and SW2 along with parallel connected auctioneering diodes allows current flow solely into the batteries from power DC bus. It allows the direct voltage input ranging from 300V up to 700V and with use of one phase inverter changes current into 21 kHz quasi-sinusoidal waveform.

High frequency is needed to avoid the typical noise and then is transformed with use of high-frequency transformer of 1.87 voltage ratio. This unusual ratio value ensures almost trapezoidal/square voltage waveform which in turn creates minimal amount of higher order harmonics what makes system more efficient. The core of power flow control is achieved by input/output square voltage phase shift control and with use of presented dual-active bridge it can work with minimal set of voltage and current measurements.

Preprints.org (www.preprints.org) | NOT PEER-REVIEWED | Posted: 1 February 2024 doi:10.20944/preprints202402.0061.v1



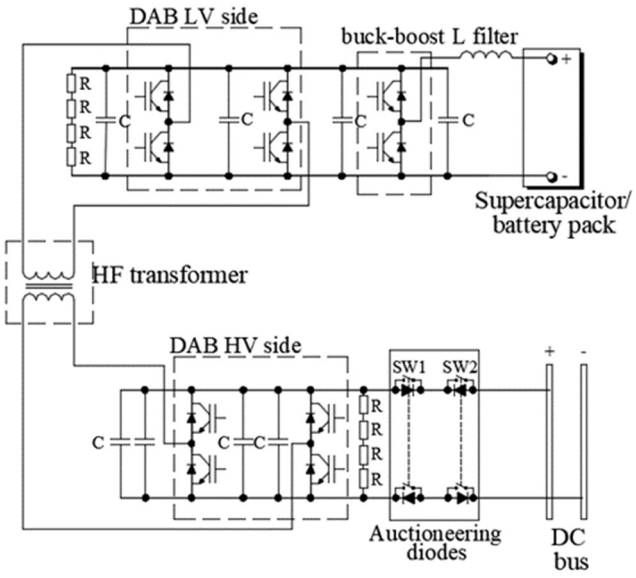


**Figure 12**. Circuit of bidirectional DC-DC converter with high frequency transformer and auctioneering switch module.

*2.5. Diode recovery current and ringing effect*

To verify the validity of the assumptions regarding the use of auctioneering diodes in the power distribution system, appropriate circuits were created in simulation software.

The prepared layout was put together from elements that had the detailed parameters of real semiconductor devices. The entire simulation rig is shown in Figure 13.

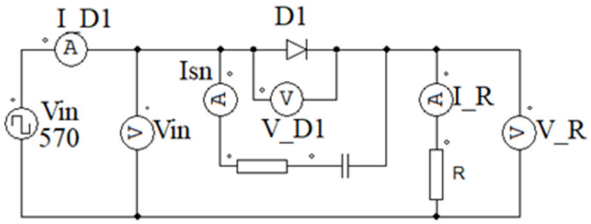


**Figure 13**. Simulated system including direct voltage source Vin (passive) with diode D1.

First, to recall how the diode conducts and gets into off state it is important to realize that these processes are not instant, and the diodes are not ideal switches. There are few important parameters such as recovery time which occurs during transition to off state.

After forward current flow, reverse current flows for a moment when reverse voltage is applied to the diode. The result of this reverse current flow is referred to as recovery current. When conducting forward current, all junction diodes store charge in the form of excess carriers. Minority carrier injection is a conductivity modulation mechanism causing the forward voltage to drop, which is favorable in this case.

The stored charge must be removed or neutralized in the PN junction before the diode gets to the off state while diode commutation process. Reverse recovery time is the amount of time it takes for this to happen $t_{rr}$ and is made up of two different intervals denoted in the Figure 14 as $t_a$ and $t_b$.

 doi:10.20944/preprints202402.0061.v1



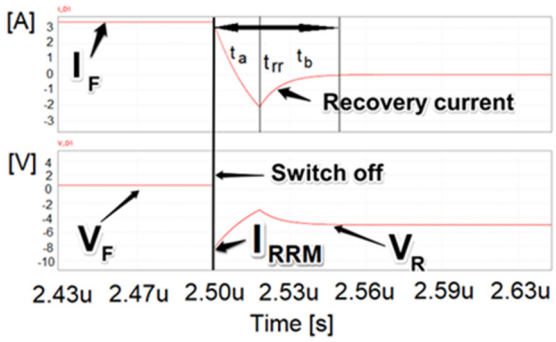


**Figure 14**. Simulation results and the waveforms of forward current $I_F$ and voltage $V_F$ obtained while switching off process. The $t_{rr}$ depicts diode's recovery time and $I_{RRM}$ is maximum reverse recovery current.

A diode that conducts forward current has a corresponding forward voltage drop $V_F$ and a stored electrical charge proportional to the forward current. Recombination process neutralizes a portion of the internal stored charge when the diode current commutates. Recombination process and reverse current $I_{rr}$ flowing across the diode and associated circuit parts diminish the remaining stored charge.

The forward current $I_F$ eradicates at a rate di/dt defined by the circuit inductance and the applied voltage while commutation process in the diode. When the diode current drops to zero, stored electrical charges force flow of the reverse current until the diode junction area is totally depleted.

The voltage drop across the diode is still positive throughout this section of $t_{rr}$, but it is smaller than the value of $V_F$ during forward conduction. In typical diodes, the current flowing during $t_a$ can be substantial. As a result of the low voltage drop across the diode, the diode's power dissipation during $t_a$ can be considered as minor. The semiconductor element, on the other hand, may have a large power dissipation because it carries the full diode reverse current while supporting the circuit's full voltage. A diode with a smaller reverse current allows work at a lower temperature.

The voltage across the diode rises from a small positive value to the entire reverse voltage applied during this time. During $t_b$, there is significant power dissipation in the diode due to the simultaneous reverse current flow and high voltage drop across it. To reduce power loss during this time, one may infer that the diode with the shortest $t_b$ should be used. The area under the current-time curve during $t_{rr}$ is defined as the total reverse recovered charge left denoted often as $Q_{rr}$. The energy that must be expended in the power switching side of the circuit is represented by this charge.

Another common problem in diode switching process is so-called ringing of recovery reverse current shown in the Figure 15. This process can be observed under unfavorable combinations of commutating current rapid increases, circuit stray inductance, forward current small value and in the case of low p-n junction temperature. As a result of snappy recovery, all fast switching power diodes produce excessive voltage spikes [22]. The operation of the presented system and its components is burdened with disadvantages as heat losses. Some calculations may be used to predict conduction and off-state losses in the junction which have a significant impact on diode power dissipation and junction temperature levels.

 doi:10.20944/preprints202402.0061.v1



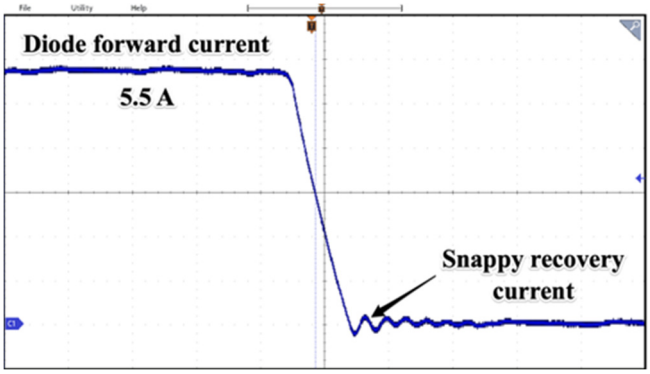


**Figure 15**. Waveform of Y50ZPD-22-24 rectifier diode's snappy recovery time current. Time base 1 ms/div.

The diode's total power losses can be computed as sum of conducting, off-state and switching losses.

The conducting state losses can be expressed as:

$$P_c = V_F \cdot I_F \cdot \frac{t_{on}}{T} \tag{20}$$

As the off-state losses are given by:

$$P_{Off} = V_R \cdot I_R \cdot \frac{t_{off}}{T} \tag{21}$$

Finally, the switching losses are as follows:

$$P_{SW} = Se_{rr} \cdot f \tag{22}$$

Where $Se_{rr}$ is switching energy losses due to reverse recovery and $f$ refers to the switching frequency.

Due to the complexity of diode dynamic recovery characteristics determining switching losses is quite difficult. In most of the applications the total charge associated with diode recovery represents energy that will be dissipated among various components of the circuit and can be expressed as:

$$Se_{rr} = \int_0^{t_{rr}} I(t) \cdot V(t) dt \tag{23}$$

Due to the principle of operation of the presented system the determination of losses using (23) is very complicated mainly because of the nonlinear voltage-current characteristics of power electronic switches (diodes) and it will not be the subject of this paper.

As will be shown in the following sections, the operation of the proposed system depends mainly on the switching phenomena of auctioneering diodes. According to (22) the energy losses and heating of diodes will depend greatly on the switching frequency, which is directly depends on the working frequency of the control system. These losses are hard to predict due to independent control of parallel connected subsystems.

### *2.6. Simulation results of proposed dc multipoint distribution system*

To verify assumptions regarding use of auctioneering diodes the numerical simulation system was prepared and deployed under different conditions. To minimize oscillations (ringing) caused by switching-off diodes the RC snubbers were introduced. Most of unwelcome voltage spikes and ringing can be observed on voltage waveforms across auctioneering diodes. One of the methods partially eliminating these situations is snubbers use connected in parallel with diodes.

These RC series connected snubbers provide a significant amount of protection for power electronics components (transistors, diodes etc.) as well as reducing EMI, particularly in switching applications.

Preprints.org (www.preprints.org) | NOT PEER-REVIEWED | Posted: 1 February 2024 doi:10.20944/preprints202402.0061.v1



In power electronics, resistor-capacitor (RC) networks are commonly used to reduce voltage spikes caused by parasitic capacitances and inductances in transformer, inductors, diodes, transistors, and systems, allowing transistors and diodes to handle more power.

Because of a mutually resonant relationship between inductances and capacitances, those spikes can cause EMI/EMC problems with both conducted and radiated emissions.

In situations where RC snubbers cannot be used, resistors or ferrites are used to introduce losses, especially when the ringing frequency is not significantly different from the switching frequency.

As illustrated in Figure 16, the snubber RC is made up of two components combined in parallel with diodes. Such a solution is often used in switching applications like inverters and DC/DC converters.

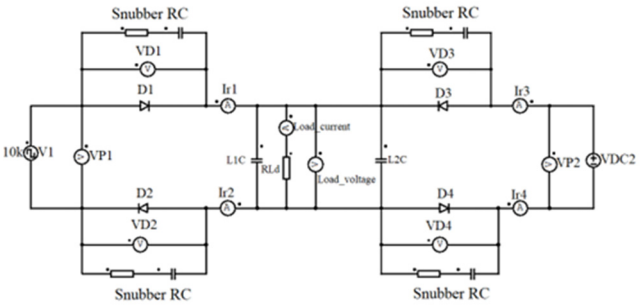


**Figure 16**. Simulated system with RC snubbers including direct voltage source VDC1 (passive) and active VSQ1, pulse voltage source connected through identical auctioneering diodes D on both positive and negative branches.

Usually, the proper values of RC ladder must be determined with experimental procedures and/or by trial and error with a real prototype. The ringing problem is related to parasitic parameters (e.g. inductance), so simulation results alone cannot be used to optimize the proper values of filtering elements. The procedure leading to the determination of the snubber resistance value can look like the following. First it is necessary to know value of the ringing frequency to calculate snubber resistance in a way that it adds some losses needed for oscillations disperse. The ringing in such circuits is related to underdamped resonance which comes from very low energy losses so the solely capacitance is not enough for snubber applications. The needed frequency can be taken from oscilloscope waveform and analyzed. Then it is convenient to measure self-inductance of circuitry and calculate capacitance of the snubber. Another method that helps with snubber parameters determination is parallel connecting capacitors $C_p$ of different values to reduce ringing frequency to half of the original value. Then it is possible to calculate snubber capacitance $C_{sn}$ as a third part of chosen capacitance according to following:

$$C_{sn} = C_p/3 \tag{24}$$

From the equation of resonant frequency, the inductance of circuitry can be calculated as:

$$L_s = \frac{1}{(2\pi f_r)^2 \cdot C_{sn}} \tag{25}$$

And knowing of that the characteristic impedance of circuitry can be expressed as:

$$Z = \sqrt{L_s \cdot C_{sn}} \tag{26}$$

The snubber resistance in this case should be equal to the calculated impedance. To avoid direct current flow across shunt snubber resistor there should be added in series capacitor which filters out higher frequencies but at the same time introduces losses. From such the bigger capacitance the higher losses so the value of it should be chosen carefully. The values needed for snubber calculations were taken by measurements of the application elements later utilized in experimental tests. Based on obtained values the numerical setup was prepared in which the snubberless system consisting of the exact same auctioneering diodes was implemented and simulation tests performed. For

 doi:10.20944/preprints202402.0061.v1



comparison the same circuit was created but with RC snubber and launched. The simulation software used nonlinear, exact diode models in which transient states and recovery current were implemented. The recovery currents described in the previous chapter were lasting from nanoseconds to even microseconds [23] and in anti-parallel connection occurred a negative current flow.

Simulation tests containing diodes with different recovery times, different sampling frequencies of sources as well as RC snubbers and L-smoothing filters were performed and chosen results were presented in the Figure 17.

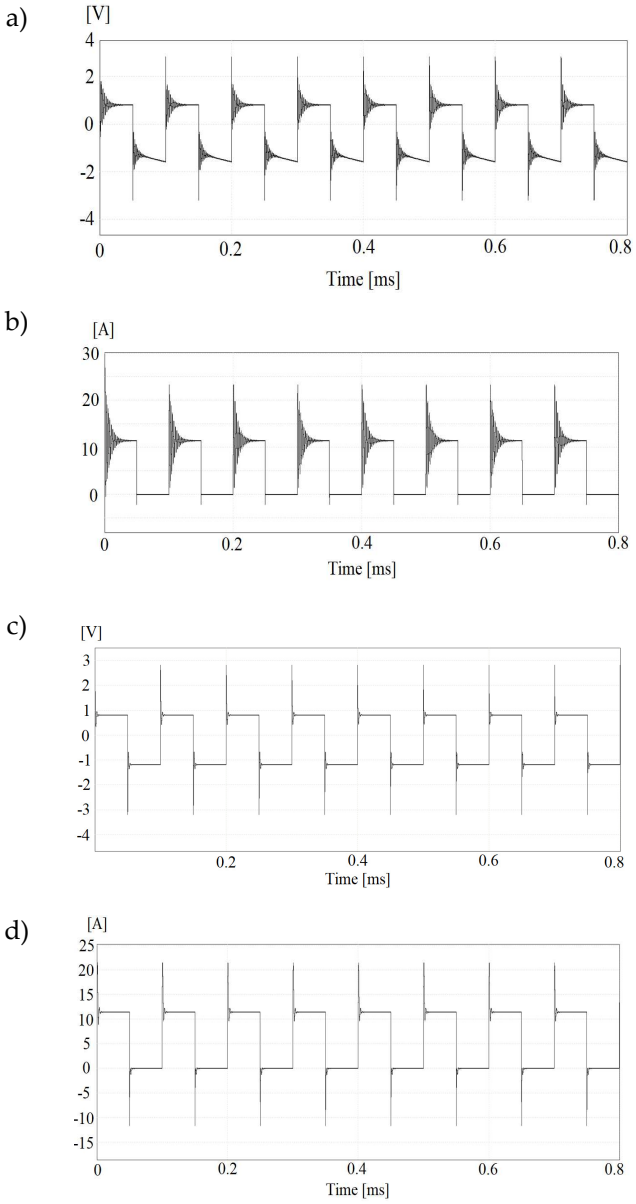


**Figure 17**. The waveforms of voltages drop and currents across the auctioneering diodes. Simulation results regarding system without snubbers (Figures a, b) and utilizing RC snubbers (Figures c and d).

In the Figure 18a there is current waveform acquired in snubberless circuit while in Figure 18b is presented situation in a case of snubbers presence. The operation of the voltage sources in the proposed system with auctioneering diodes was also checked. In addition to providing information on the values of charging and discharging currents of the supercapacitor, the simulation tests revealed limitations of the system. Due to the nonlinear nature of the fast charging process of supercapacitors, the simulation results were used to select the capacitor current controllers in such a

 doi:10.20944/preprints202402.0061.v1



way that they don't exceed the permissible currents values generated by the machine inverter while maintaining stability of operation.

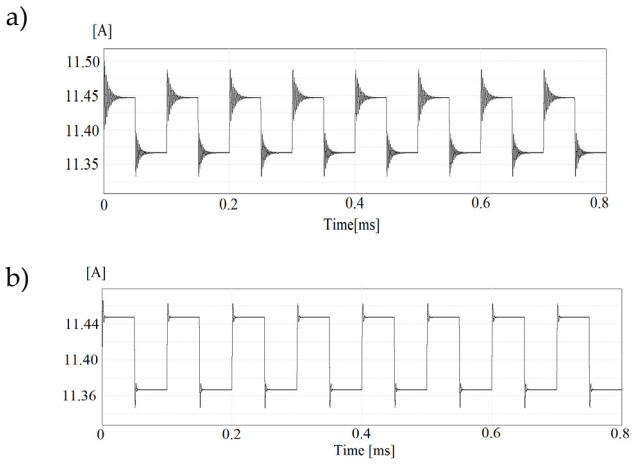


**Figure 18**. The waveforms of currents across the electrical load.

As a result of the analysis of results, there are important factors to consider when it comes to power distribution in DC grids. Among them is the use of RC snubbers in conjunction with diodes. While switching between diodes, a high ratio of current raise di/dt can cause a lot of stress on semiconductors, so a proper filtering system is essential to avoid this issue. Due to high switching frequency the inner structures of auctioneering diodes are also unavoidably heated thus high power control algorithms must consider this phenomenon and change switching frequency with means of changing gains in PI controllers. It can be concluded that there is a complete control over the power distribution process in the DC grid.

### 3. The experimental set up and results

The laboratory test rig consists of an internally transformer-isolated 7 kVA DC-DC converter and a 7 kVA AC/DC converter that draws power from a synchronous generator. The 5.5 kW synchronous self excited machine is driven by a MMG50SR120B IGBT module. Using parallel connected intermediate circuit capacitors, the total capacitance equals to 200 µF and can withstand a maximum voltage of 1200 V. The switching frequency was set at 20 kHz due to the relatively small power of the loads. The DC-DC converter is based on CAS120M12 SiC transistor half bridges. The boost-back converter operates at 21 kHz, while the bridges operate at 25 kHz. The supercapacitor used was Maxwell BMOD0165 P048 with nominal capacitance 165 farads at 48 volts.

For voltages measurements, an LEM CV 3-1000 transducers were used. When mounted on heat sinks, all auctioneering diodes were 16FR120Ms, capable of withstanding 1200 volts with 16 amps of continuous current. Direct current two-pole contactors controlled by a PLC were used to connect the electrical consumers. DC-DC converters and machine inverters were equipped with their own DSP-FPGA controllers. The control units consisted of a SH363 processor board with an ADSP21363 digital signal processor, which was controlled by software. DSPs were used for processor subroutine control programs, while FPGA board calls were made via processor subroutines. Analog to digital converters were incorporated into FPGA boards, and input signals were directed to DSPs through isolated transducers. Through dedicated hardware drivers, the FPGA controlled the IGBT transistors gating. The energy management control board was based on the SH363 type processor and controlled both machine and energy storage converters control boards. There are an input/output ports on the FPGA board which are electrically compatible with an industrial Modbus RS485 two-wire port. Modbus communication lines have been equipped with optoisolation gates to reduce electromagnetic interference, resulting in a significant improvement in the quality of the transmitted data frames.

 doi:10.20944/preprints202402.0061.v1



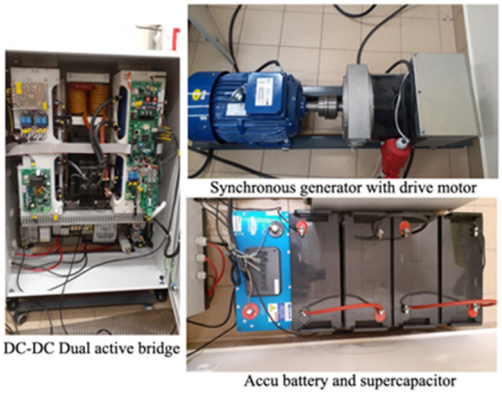


**Figure 19**. Overview of investigated laboratory setup.

For the data acquisition the 4 channels digital MDO3 200MHz, oscilloscope in the Hi Res mode was used. The oscilloscope waveforms were taken at a time base of 2 s/div unless otherwise noted. It was demonstrated that the power sharing feature of the presented system can be used in both battery and supercapacitor discharge and charging modes. Supercapacitors were initially charged to 43 volts, leaving safety limits for possible overvoltage spikes. After the line side inverter was turned on, power was delivered to the DC grid through auctioneering diodes and closed switch S2 thanks to the phase shift introduced by the storage system inverter.

High frequency transformer circuitry operated in discharging mode was equipped with auctioning diodes and current bidirectional switches (denoted as SW in Figure 12) to prevent reverse current flow from the DC bus to the primary winding. The DC voltage value at the output of the grid-side converter was set to 570 V and maintained by the control loop of the DC-DC converter. In addition, there was a direct current limit applied to control loop as not to exceed its nominal value. The inverter's intermediate circuit's voltage has been changed and a proper current limit has been applied to an energy management system for controlling the DC bus synchronous generator's power output. A DC-DC converter voltage was applied to the DC busbar, and then known electrical load was switched on. Power electronics control system was able to control power sharing by changing DC bus voltage precisely. Power sharing operation and voltage quality can be improved by altering the DC-DC converter output voltage at the same time, but for simplicity only the machine inverter side voltage was used.

Just for comparative purposes in the Figure 20 there are three drawings acquired for the system with cascaded PI regulator and a current waveform depicting operation of the earlier version of the system presented in [4] without cascaded controller.

a)

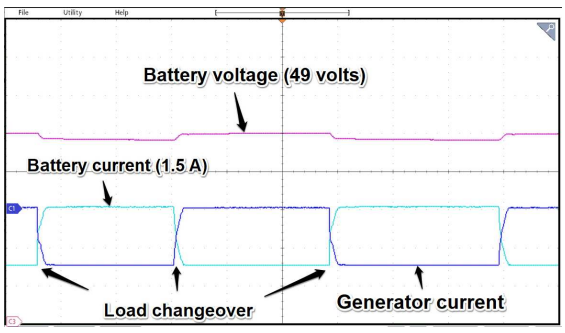

Preprints.org (www.preprints.org) | NOT PEER-REVIEWED | Posted: 1 February 2024 doi:10.20944/preprints202402.0061.v1



b)

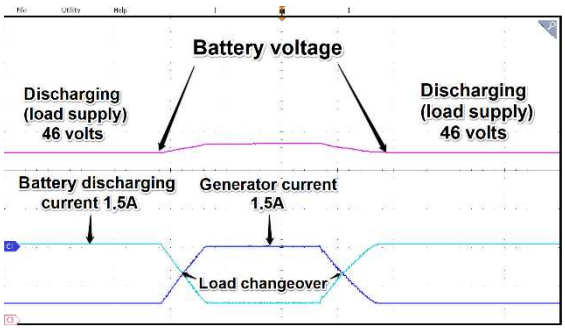


c)

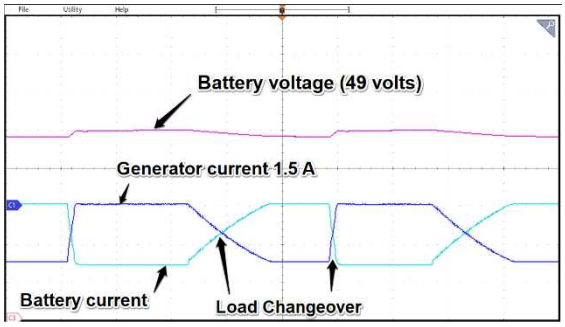


**Figure 20**. Waveforms of currents and battery voltage while load changeover with (Figure a, b) and without (Figure c) cascaded controller operation. Time base 2 s/div.

It is clearly seen in Figure 20c that for given parameters reaching a power distribution steady state settling time after load changeover is much longer due to the system's main controller settings. It can be noticed that in version without additional PI controller there is no possibility to change dynamics of the load sharing process and is mainly based on the instantaneous values of the voltages at the terminals of the generator converter and the DAB.

a)

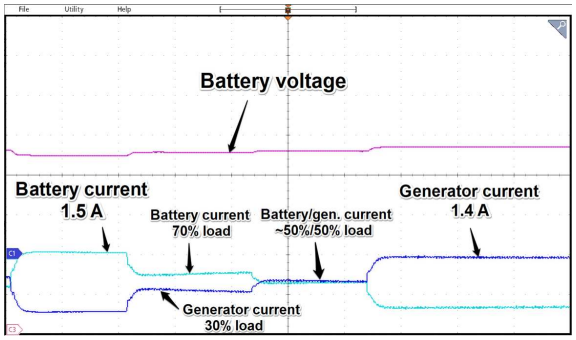


b)

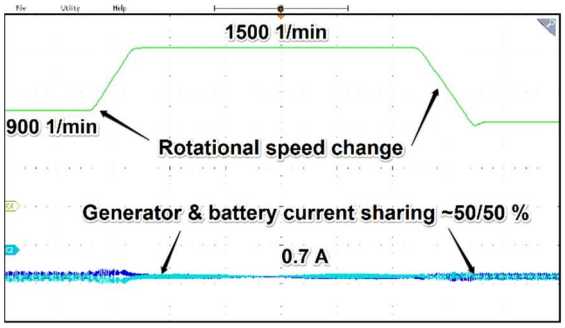


**Figure 21**. Waveforms of currents and battery voltage while power sharing operation with 800W resistive load. Time base 2s/div.

 doi:10.20944/preprints202402.0061.v1



As can be seen from the oscillograms in Figures 22 when the system operates in power distribution mode, the waveforms of the obtained currents are controlled continuously, but due to hysteresis loops and phenomena in the auctioneering diodes associated with current recovery ringing, their shape is not as precariously maintained as in no power distribution mode enabled. As it was stated the control of $U_{dc}$ while power distribution operation was possible thanks to the additional control loop of accurate active current limit. As it turned out during experimental research changing the active current $i_{sq}$ of the generator and inverter by 10% required a change in voltage $U_{dc}$ of about 0.3 V. It must be noted that such subtle changes cannot be achieved with means of linear gains in the single controller PI voltage loop.

a)

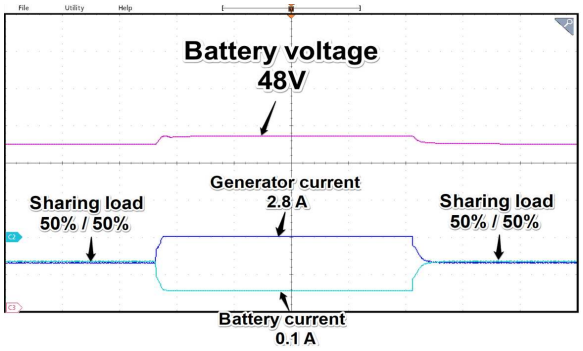


b)

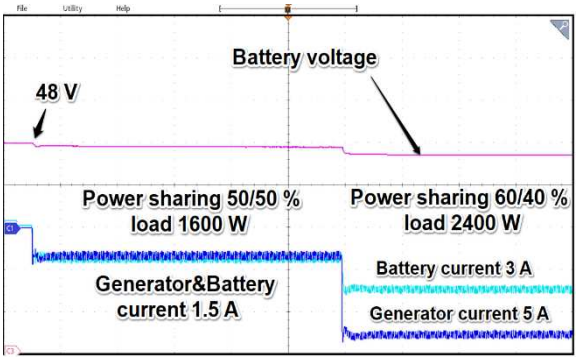


**Figure 22**. Waveforms of battery voltage drop along with battery and generator currents while different ratio power sharing operation obtained for 1600W and 2400W load. Time base 2s/div.

In the following tests the influence of battery type (battery pack or supercapacitor) was investigated. The only source of power was battery and DAB converter. The tests were performed for two different resistive loads and chosen results are presented in Figure 23. For such loads in the given time visible voltage drop on both DC sources differs of 2 volts in favor of battery which is natural due to a low energy density in the supercapacitor. In both cases the experimental results showed possibility of stable feeding consumers for a relatively short time.

a)

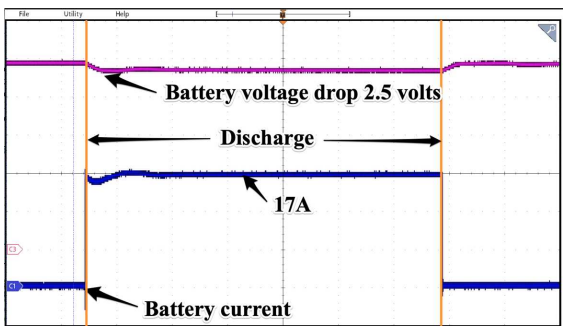

 doi:10.20944/preprints202402.0061.v1



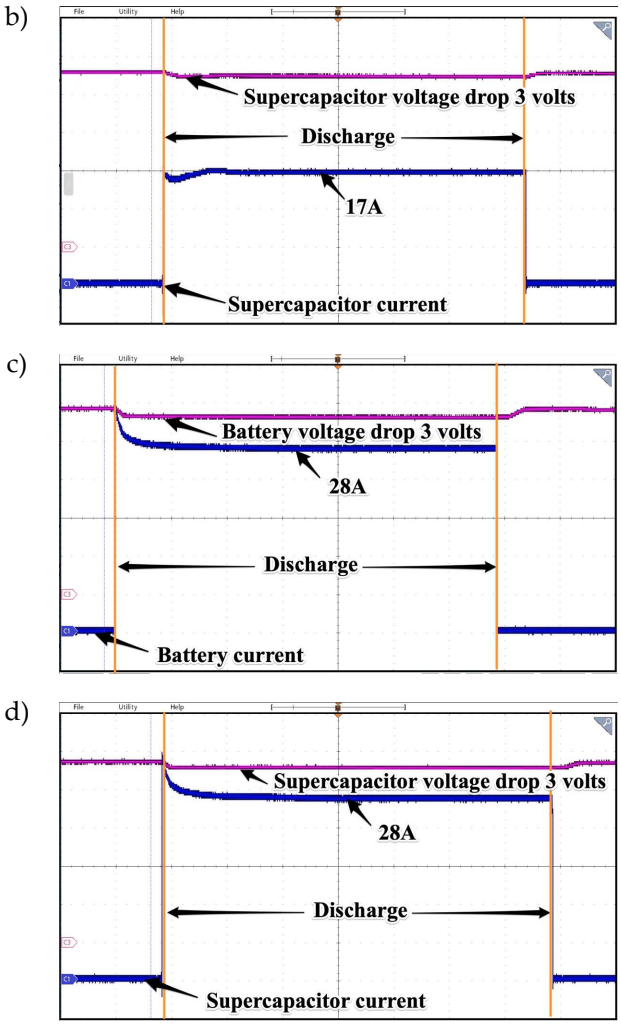


**Figure 23**. Waveforms presenting voltage drop and discharge current drawn from battery (a & c) and supercapacitors (b & d) for 800W and 1500W loads respectively. Time base 2s/div.

The difference between battery and supercapacitor bank shows up clearly in prolonged discharging operation.

Supercapacitors are different from batteries because they do not rely solely on an electro-chemical processes to function. The capacitors store potential energy electrostatically within their internal structures. To separate positive and negative charges accumulating on the plates of each side, supercapacitors use a dielectric or insulator to separate the metallic covers. The most important advantage of supercapacitors is that, compared to electrochemical batteries, the electrical properties and capacity do not change much with aging. The most serious disadvantage of modern supercapacitors is a relatively fast self-discharge process which becomes more troublesome in low temperatures.

Another important feature is faster process needed to charge and discharge supercapacitors than batteries, since they have higher power throughputs.

In terms of power density, electrochemical capacitors with high equivalent series resistance (ESR) values and time constants between one and hundred seconds are equal to batteries. The latest graphene electrode design in supercapacitors can get very close to electrolytic capacitors, which are 10 times more powerful than conventional batteries moreover they have time constants ranging from 0.1 second up to 30 seconds. In turn, this led to the conclusion that supercapacitors are most suitable for short bursts of power, as evidenced by the tests that were conducted.

As it can be seen (see Figure 24) the discharge process of 165 F capacitor is rapid and this feature clearly shows that supercapacitor should be used as an intermediate voltage source mainly for

 doi:10.20944/preprints202402.0061.v1



harvesting peaks or as a buffer for the battery. Long time operation should be performed with use of batteries which have higher energy density thus some software means should be provided to ensure dynamic power distribution between voltage sources while operation. It can be also considered as a form of prebuffer which decreases number of charge/discharge operation on electrochemical batteries when frequent deep cycling shortens their operational lifespan.

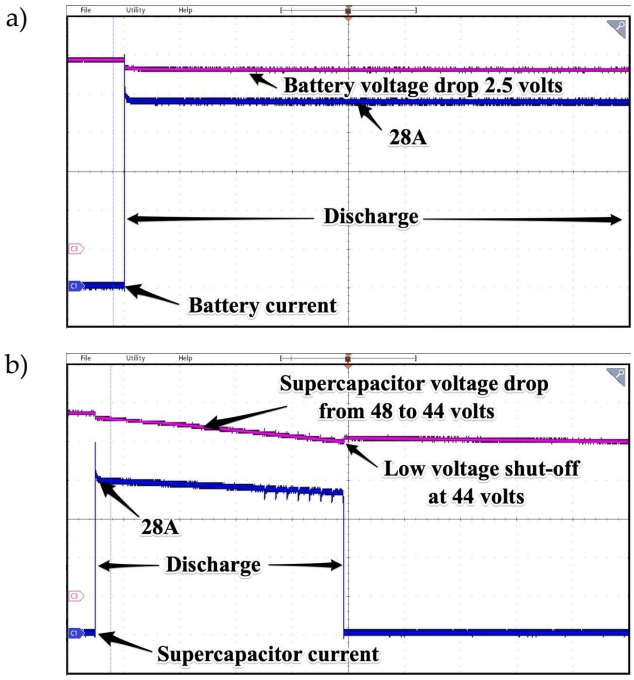


**Figure 24**. Prolonged discharging process of electrochemical battery (a) and supercapacitor (b). Test lasted 90 seconds for 1500W load. Time base 2s/div.

Next test of charging batteries and supercapacitor was performed to check times needed for full charging. The bidirectional switches and DAB were set to charging mode. In the charging mode buck-boost converter drops the voltage to level above batteries nominal value. This setpoint can be changed due to needs because all parameters of controller are easily configurable. In the proposed solution system can work together with batteries management system or can be controlled by external energy management system by means of Modbus communication protocol.

As it can be observed in the Figure 25a the tests covered charging batteries with different currents which values were gradually increased. Along with changes in charging current, the SESG current also increased. Its value was inversed just for clarification the picture.

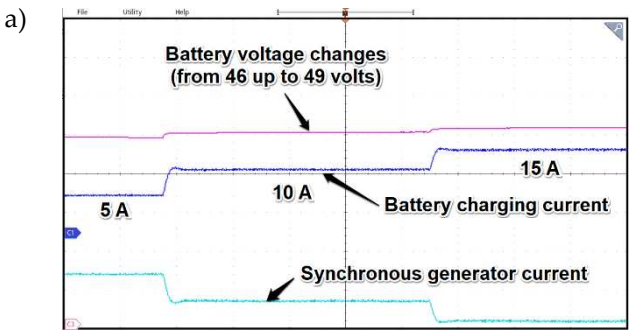

 doi:10.20944/preprints202402.0061.v1



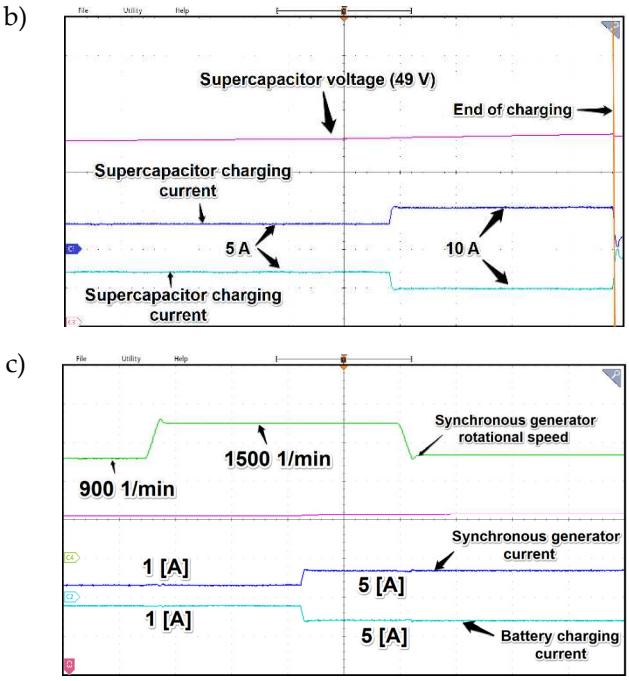


**Figure 25**. Waveforms depicting charging process of electrochemical battery (a) and supercapacitor (b) along with rotational speed change influence on DC bus voltage and currents (c). Time base 2 s/div.

In the Figure 25b there are waveforms of the supercapacitor voltage, charging current and generator current. As expected, the charging process is very fast in this case, but the voltage value should be carefully controlled because overcharging the supercapacitor can lead to damage. The control system of charging process is set in a way that it controls the voltage in 5 seconds period and in the case of signal error there is charging process enabled. This is manifested by current peaks appearing at regular intervals what is depicted in the Figure 24b. The maximum value of the charging current pulses is software-defined and can be changed according to the needs of the application. These current peaks clearly show one of the disadvantages of supercapacitors mentioned earlier, that is, the natural process of relatively quick self-discharge. The tests regarding charging processes proved that the same as for discharging the supercapacitor works best as the buffer between energy storage (batteries) and DC grid. The charging process is quick and can be used for rapid electrical energy harvesting so these energy storage devices can work mainly as a buffer between DC grid and batteries bank.

The last subplot denoted as 25c presents influence of speed change on battery voltage and charging current along with SESG current. Thanks to field oriented control the direct current is not changing notably what was one of the goals of presented application. As the results of subsequent tests proved, the change in active current $i_{sq}$ of the generator is noticeable difference during changes in speed namely for low RPM's the current increases while in the case of high speed the active current value drops. However, as long as the value of the dc bus voltage is stabilized in varying rotational speed operating states expected power distribution was preserved as well.

## 4. Conclusions and further work

An article presents selected results of a charge/discharge supercapacitor converter system consisting dual active bridge connected to the battery/supercapacitor working in parallel connection with self excited synchronous generator inverter. The main goal of presented project was to improve response time of the existing system through adding additional controller which action can be observed in the Figure 20. The additional cascaded controller allow much faster and precise control of transient process for power changeover operation which resulted settling time of 0.33 s instead of 2.40 s for the 800 W and 1600 W load changeover from generator to battery supply. Presented solution

allows to control power changeover time in both directions, which feature is required in the case of power sharing industrial applications. Further work, including optimization of controllers to obtain even faster power changeover according to ramp change will be undertaken. It is proposed to carefully select and tune snubbers which will improve the quality of generated energy, especially when operating in parallel. As a final improvement, a lithium-ion battery pack will be connected, and an auctioneering diodes automatic switching communicating with energy management unit system will be incorporated.

**Author Contributions:** Conceptualization M.K.; methodology M.K.; software M.S.; validation M.K. and S.S.; formal analysis M.K.; investigation M.K.; resources M.K.; data curation S.S.; writing—original draft preparation M.K.; writing—review and editing M.K.; S.S.; M.S; visualization M.S.; supervision M.K.; project administration M.K.; funding acquisition M.K. All authors have read and agreed to the published version of the manuscript.

**Funding:** Please add: This research was funded by Polish Ministry of Science and Higher Education, grant number 1/S/KEiE/2023.

**Conflicts of Interest:** The authors declare no conflicts of interest.

## References

1. Dragičević, T.; Lu, X.; Vasquez, J.C.; Guerrero, J.M. DC Microgrids - Part I: A Review of Control Strategies and Stabilization Techniques. *IEEE Trans. on Power Electronics* **2016**, *Volume 31, no. 7*, pp. 4876-4891.
2. Jin, Z.; Savaghebi, M.;Vasquez, J.C.; Meng, L.; Guerrero J.M. Maritime DC microgrids - a combination of microgrid technologies and maritime onboard power system for future ships. *IEEE 8th International Power Electronics and Motion Control Conference (IPEMC-ECCE Asia)* **2016,** pp. 179–184.
3. Kozak, M.; Zawirski, K. A Concept of Induction Squirrel Cage Generator Application in Ship Electric Network, *IEEE 20th International Symposium on Industrial Electronics (ISIE)* **2011**, pp. 483-488.
4. Kozak, M.; Gordon, R.; Zarębski, A. Power sharing system with use of DC-DC converter and intermediate circuit of VSI inverter. *Poznan University of Technology Academic Journals - Electrical Engineering* **2020**, pp. 69-84.
5. Mirzaeva G.; Miller, D.; Mirchell S.; Steber. A. Hybrid Propulsion System for Marine Vessels based on a DC Microgrid. *2022 IEEE Energy Conversion Congress and Exposition (ECCE)*, **2022**, pp. 1-7.
6. M. Nowak, J. Hildebrandt, P. Luniewski, "Converters with AC Transformer Intermediate Link Suitable as Interfaces for Supercapacitor Energy Storage", *IEEE 35th Annual Power Electronics Specialists Conference*, Aachen, Germany, 2004, pp. 4067-4073.
7. Mutarraf M. U. A Decentralized Control Scheme for Adaptive Power-Sharing in Ships based Seaport Microgrid. *IECON 2020 The 46th Annual Conference of the IEEE Industrial Electronics Society*, **2020**, pp. 3126-3131.
8. Brown, H.E.; Suryanarayanan, S.; Natarajan, S. Improving reliability of islanded distribution systems with distributed renewable energy resources, *IEEE Trans. Smart Grid*, **2012**, *Volume 3, no. 4*, pp. 2028–2038.
9. Kozak, M. Alternating Current Electric Generator Machine Inverters in a Parallel Power Sharing Connection. *IEEE Access*, **2019**, *Volume 7*, pp. 32154-32165.
10. Carbone R. Energy Storage in the Emerging Era of Smart Grids. **2011**, pp. 161-162.
11. Vandoorn T.L.; Meersman B.; De Kooning J.D.M. Transition from islanded to grid-connected mode of microgrids with voltage-based droop control, *IEEE Trans. Power Syst.*, **2013**, *Volume 28, no. 3*, pp. 2545–2553.
12. James C. A Novel Power Sharing Control Method for Distributed Generators in DC Networks. M.S. thesis, Electrical and Computer Engineering, The Old Dominion University, 2018. Available online: https://digitalcommons.odu.edu/cgi/viewcontent.cgi ?article=1156&context=ece_etds. (accessed on 30 January 2024).
13. Ton D.T.; Wang W.T.P. A more resilient grid: The U.S. department of energy joins with stakeholders in an R&D plan. *IEEE Power Energy Magazine*, **2015**, *Volume 13, no. 3*, pp. 26–34.
14. Qing-Chang Z.; Yu Z. Parallel Operation of Inverters with Different Types of Output Impedance. *Industrial Electronics Society, IECON 2013 - 39th Annual Conference of the IEEE 2013.* **2013**, pp. 1398-1403.
15. Rules for classification of ships DNV. Newbuildings machinery and systems – main class. Electrical installations. **2016**. Available online: https://manualzz.com/doc/o/udx66/dnv-ship-rules-pt.4-ch.8---

electrical-installations-b-200-additional-requirements-for-high-voltage-assemblies. (accessed on 30 January 2024).

16. Imecs M.; Incze I.I.; Szabo C. Stator-Field Oriented Control of the Synchronous Generator: Numerical Simulation. *International Conference on Intelligent Engineering Systems INES 2008.* **2008**, pp. 93-98.
17. Baktiono S. Study of Field-Oriented Control of a Permanent Magnet Synchronous Generator and Hysteresis Current Control for Wind Turbine Application", M.S. thesis, Electrical and Computer Engineering, The Ohio State University, **2012**. Available online: https://etd.ohiolink.edu/apexprod/rws_olink/r/1501/10?clear=10&p10_accession_num=osu1338314559 (accessed on 30 January 2024).
18. Yongho L.; Sunggook O.; Sunwon P. Enhanced Control with a General Cascade Control Structure. *Industrial & Engineering Chemistry Research*, **2002**, *Volume 41, no.11*, pp. 2679-2688.
19. Saxena S.C.; Kumar V.; Waghmare L.M. Cascade Control of Interconnected System Using Neural Network. *IETE Journal of Research*, **2002**, *Volume 48, no. 6*, pp. 461-469.
20. M. P. Kaźmierkowski, H. Tunia, Automatic Control of Converter-Fed Drives, *Warsaw-Amsterdam-New York-Tokyo, PWN-Elsevier science publishers.* **1994,** 559 pages.
21. Martins F.G.; Tuning PID Controllers using the ITAE Criterion. *International Journal of Engineering Education.* **2005**, *Volume 21, no. 5*, pp. 867-873.
22. Rahimo M.T.; Shammas N.Y.A. Freewheeling diode reverse-recovery failure modes in IGBT applications. *IEEE Transactions on Industry Applications,* **2001**, *Volume 37, no. 2,* pp. 661-670.
23. Diode Model with Reverse Recovery, *PowerSim, Troy, MI, U.S.A.*. Available online: https://psim. powersimtech.com/hubfs/PDF%20Tutorials /General% 20PSIM%20Use/Tutorial-Diode-model-with-reverse-recovery.pdf (accessed on 30 January 2024).